# Effect of the Kinematic Lower Boundary Condition on the Spectral and Auto-correlation Structure of Annular Variability in the Troposphere

Torben Kunz and Richard J. Greatbatch, *GEOMAR Helmholtz Centre for Ocean Research Kiel, Kiel, Germany*, presented at AGU Fall Meeting, December 2013, San Francisco, CA, USA – Contact: tkunz@geomar.de

**[Paper number: A23F-0364]**

GEOMAR

## a. Geopotential Green's function response

Vertical Green's function response $\hat{\Phi}$, of the modified zonal mean geopotential $\sqrt{\cos\phi\,\rho_0} \times \bar{\Phi}$, to a mechanical forcing applied in a single Hough mode (with eigenvalue $\epsilon$) and concentrated at a particular level, at $z = 0$, with amplitude $\hat{f}_*$ (expressed in units of $\hat{\Phi}$ per time) and frequency $\omega$, assuming QG TEM flow with constant static stability, uniform Newtonian cooling ($\alpha =$ const) and a frictional ($\kappa_b$) rigid lower boundary (at $z = z_b$), in spherical and log-pressure coordinates (following Garcia 1987, Haynes and Shepherd 1989, Haynes et al. 1991):

$$\hat{\Phi} = \begin{cases} B_\times^>\hat{\Phi}_0 \exp(-\Lambda z) & \text{at} \quad z > 0 \\ B_\times^<\hat{\Phi}_0 \exp(+\Lambda z) & \text{at} \quad z < 0 \end{cases}, \qquad (1)$$

with

$$\Lambda = \left(\gamma + \frac{1}{4H^2}\right)^{1/2}, \quad \gamma = \frac{1}{{H_R}^2}\left(\frac{i\omega}{i\omega+\alpha}\right), \quad \frac{1}{{H_R}^2} = -\epsilon\frac{N^2}{4\Omega^2 a^2},$$

with the Green's function coefficient $\hat{\Phi}_0$ for an infinitely deep atmosphere

$$\hat{\Phi}_0 = \frac{H\gamma\,\hat{f}_*}{2\Lambda\, i\omega}, \quad \text{and} \quad B_\times^> = B\exp(2\Lambda z_b) + 1, \quad B_\times^< = B\exp(2\Lambda(z_b - z)) + 1,$$

and

$$B = \frac{\Lambda + (2H)^{-1} - \gamma(M^2 + \kappa_b/i\omega)H}{\Lambda - (2H)^{-1} + \gamma(M^2 + \kappa_b/i\omega)H}, \quad M^2 = \frac{4\Omega^2 a^2}{-\epsilon}\frac{1}{RT_{0b}}.$$

## b. Power spectra

- White noise mechanical forcing (i.e. assuming $|\hat{f}_*(\omega)| =$ const)
- Infinitely deep atmosphere ($B_\times^>, B_\times^< \to 1$ as $z_b \to -\infty$):

$$S(\omega; z) = |\hat{\Phi}_0|^2 |\exp(-\Lambda|z|)|^2. \qquad (2)$$

- Locally at $z = 0$ [i.e., $E = \exp(-\Lambda|z|) = 1$]:

$$S(\omega; z=0) = \frac{c}{4}\left(\frac{|\hat{f}_*^2|}{1+(4c)^{-1}}\right)\left((\omega^2 + \alpha_L^2) + \frac{\omega\alpha}{1+(4c)^{-1}}\right)^{-1}, \qquad (3)$$

with $c = H^2/{H_R}^2$. If $c$ small, local red noise approximation:

$$S_L(\omega) = \frac{2\sigma_L^2\alpha_L}{\omega^2 + \alpha_L^2}, \qquad (4)$$

with effective damping rate $\alpha_L$ and variance $\sigma_L^2$

$$\alpha_L = \alpha(1+4c)^{-1/2}, \quad \sigma_L^2 = \frac{c}{4}\left(\frac{|\hat{f}_*^2|}{1+(4c)^{-1}}\right)\frac{1}{2\alpha_L}.$$

- Remote red noise approximation that fits (2) at low- and high-freq.:

$$S_R(\omega; z) = \frac{2\sigma_R^2\alpha_R}{\omega^2 + \alpha_R^2}, \qquad (5)$$

with (where $E_0$ and $E_\infty$ denote low- and high-freq. limits of $E$)

$$\alpha_R(z) = \alpha_L E_\infty/E_0, \quad \sigma_R^2(z) = \frac{c}{4}E_\infty^2\left(\frac{|\hat{f}_*^2|}{1+(4c)^{-1}}\right)\frac{1}{2\alpha_R}.$$

- Effect of frictional rigid lower boundary:

$$S(\omega; z) = \begin{cases} |B_\times^>|^2|\hat{\Phi}_0|^2|\exp(-\Lambda z)|^2 & \text{at} \quad z > 0 \\ |B_\times^<|^2|\hat{\Phi}_0|^2|\exp(+\Lambda z)|^2 & \text{at} \quad z < 0 \end{cases}. \qquad (6)$$

- Red noise approximation that fits (6) at low- and high-freq. then becomes:

$$S_B(\omega; z) = \frac{2\sigma_B^2\alpha_B}{\omega^2 + \alpha_B^2}, \qquad (7)$$

with

$$\alpha_B(z) = \begin{cases} \alpha_R(z)B_{\times\infty}^>/B_{\times 0}^> & \text{at} \quad z > 0 \\ \alpha_R(z)B_{\times\infty}^</B_{\times 0}^< & \text{at} \quad z < 0 \end{cases}$$

and

$$\sigma_B^2(z) = \begin{cases} \frac{c}{4}B_{\times\infty}^{>2}E_\infty^2\left(\frac{|\hat{f}_*^2|}{1+(4c)^{-1}}\right)\frac{1}{2\alpha_B} & \text{at} \quad z > 0 \\ \frac{c}{4}B_{\times\infty}^{<2}E_\infty^2\left(\frac{|\hat{f}_*^2|}{1+(4c)^{-1}}\right)\frac{1}{2\alpha_B} & \text{at} \quad z < 0 \end{cases}.$$

where $B_{\times 0}^>$, $B_{\times 0}^<$, $B_{\times\infty}^>$, $B_{\times\infty}^<$ denote low- and high-freq. limits of $B_\times^>$ and $B_\times^<$.

## c. ACFs, timescales and variances

- True ACFs obtained numerically as inverse Fourier transform of power spectra
- Red noise ACFs given by $\exp(-\alpha_{L,R,B} \times |\text{lag}|)$
- True $e$-folding timescales obtained by linear interpolation from ACF
- Red noise $e$-folding timescales given by $\alpha_{L,R,B}^{-1}$
- True variances obtained by numerical integration of power spectrum from $-\infty$ to $+\infty$
- Red noise variances given by $\sigma_{L,R,B}^2$

## 1. Abstract

The dynamical origin of the spectral and auto-correlation structure of annular variability in the troposphere is investigated by a deductive approach. Specifically, the structure of the power spectrum and auto-correlation function of the zonal mean geopotential is analysed, for the case of a quasi-geostrophic spherical atmosphere subject to a white noise mechanical forcing applied in a single Hough mode and concentrated at a particular level in the vertical, with vertically uniform Newtonian cooling and Rayleigh drag concentrated at a rigid lower boundary. Analytic expressions for the power spectrum are presented together with expressions for an approximate red noise, i.e. a Lorentzian shaped power spectrum. It is found that for an infinitely deep atmosphere the power spectrum can be well approximated by a red noise process for the first few Hough modes (associated with large Rossby heights), provided the distance from the forcing is not larger than about one Rossby height. When a frictional rigid lower boundary is included, however, the approximation is generally bad. The high-frequency part of the power spectrum exhibits near exponential behaviour and the auto-correlation function shows a transition from a rapid decay at short lags to a much slower decay at longer lags, if the thermal and mechanical damping timescales are sufficiently well separated. Since observed annular variability exhibits the same characteristics, the above results lead to the hypothesis that these characteristics may, to some extent, be intrinsic to the linear zonal mean response problem—although the need for an additional contribution from eddy feedbacks is also implied by the results.

## 2. Structure of analytic solution

Examples for Hough mode n=4 (for which H ~ $H_R$), an isotherm. atmosph. at 240 K (i.e. H=7km, $N^2$=4x10$^{-4}$s$^{-2}$), $\alpha^{-1}$ = 20 days, $\kappa_b^{-1}$ = 1 day. ——— = true, – – – – = red noise approximation

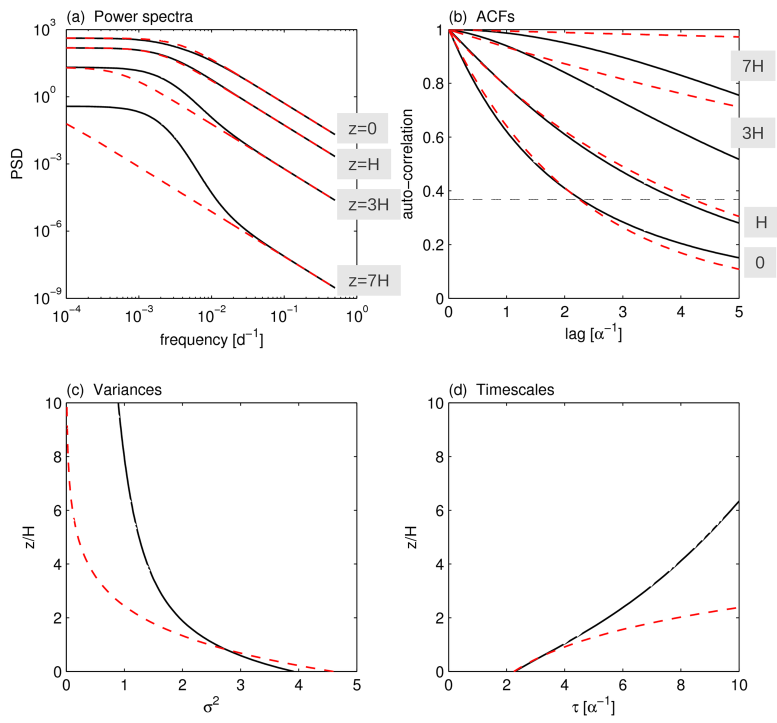

**Fig. 1:** Infinitely deep atmosphere:

- within a distance of about one Rossby height, red noise approx. provides good fit to spectrum and ACF (timescale)
- at larger distance, red noise approx. underestimates the variance at intermediate frequencies
  - ➡ underestimation of width of zero freq. spectral peak
  - ➡ overestimation of width of lag-zero ACF peak
  - ➡ red noise timescales too long
  - ➡ ACF increasingly differs from an exponential decay

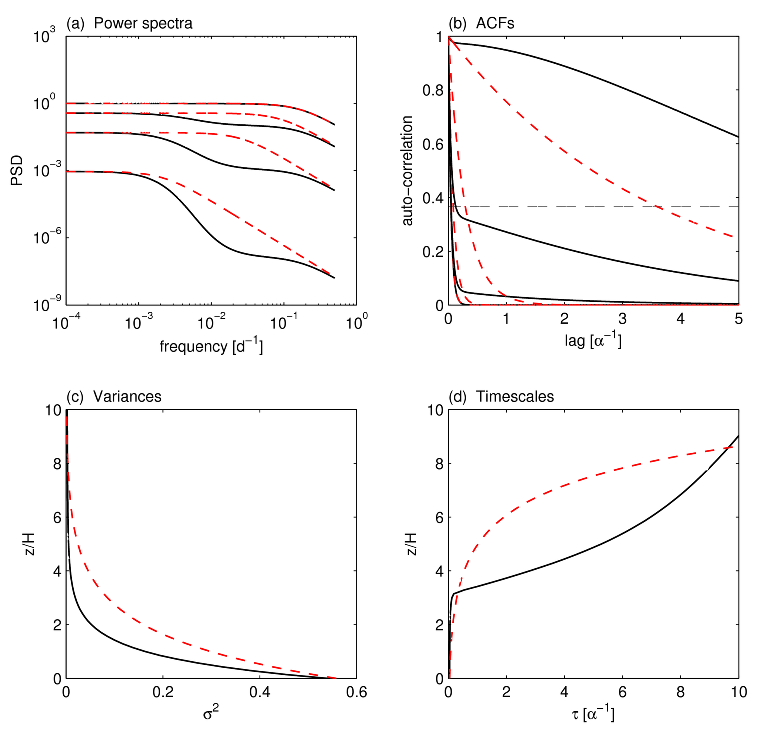

**Fig. 2:** Frictional rigid lower boundary at $z_b$ = 0:

- only very near forcing, red noise approx. provides good fit
- away from forcing red noise approx. overestimates variance at intermediate frequencies
- ACF far from exponential behaviour
  - ➡ distinct timescale behav. (superpos. of 2 components)
  - ➡ rapid decay at short lags (fast component)
  - ➡ slow decay at long lags (slow component)
  - ➡ decorrel. timescale exhibits sudden jump with height

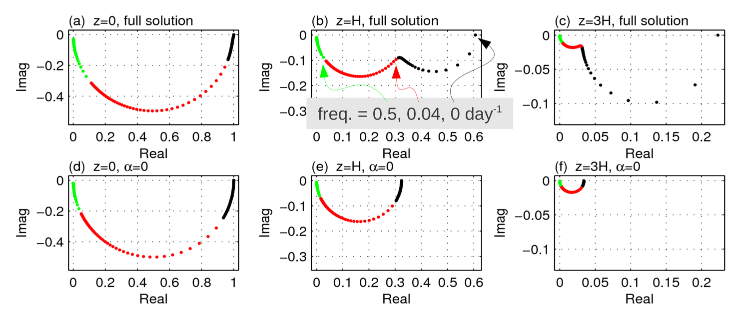

**Fig. 3:** Complex solution [Eq. (1)] for case of Fig. 2:

- top row shows full solution including thermal damping
- bottom row shows thermally undamped component (α = 0)
- ratio of fast to slow comp. decreases with height (diff. Λ's)

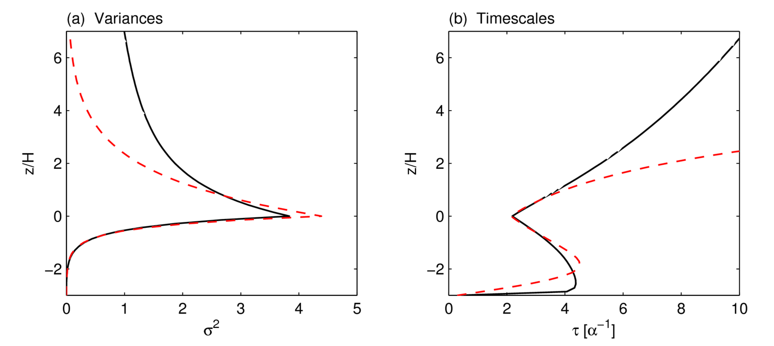

**Fig. 4:** As Fig. 2, but with boundary at $z_b$ = -3H

- effect of boundary is weak, relev. only near boundary itself
- maximum in timescale between forcing and boundary
- but near zero variance due to density stratification

## 3. Idealized tropospheric scenario

Example with two forcings, located at:

(a) z = 0 km ➡ representing near surface eddy forcing (mainly vertical EP-flux div.)

(b) z = 8 km ➡ representing upper trop. momentum forcing (mainly horizontal EP-flux div.)

with, for simplicity:

- equal amplitudes and equal spectral properties, i.e. both white noise or both weakly red noise (τ = 1 day)
- perfectly correlated in time (i.e., power spectrum obtained from sum of the two solutions), but similar results when assuming fully anti-correlated or uncorrelated forcings

Parameter setting as before, except for H = 8 km and $N^2$ = 1.5 x 10$^{-4}$ s$^{-2}$, with lower boundary (LB) at $z_b$ = 0

– – – – = white forcing, no LB, – – – – = white forcing, with LB, ——— = red forcing, with LB

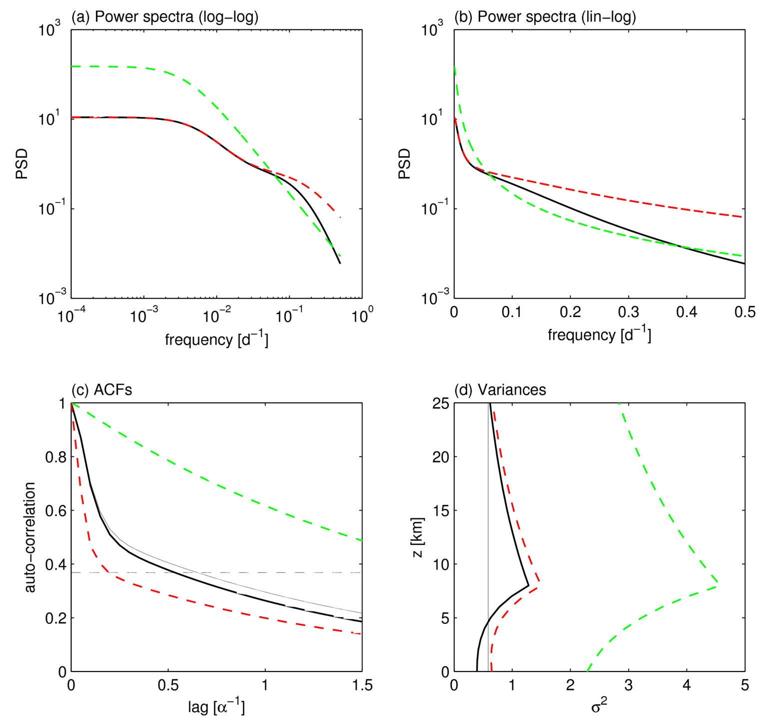

**Fig. 5:** Superposition of two forcings:

- thick lines: full solution (at z = 5 km), thin lines: barotr. comp.
- **without frictional rigid lower boundary**
  - ➡ Lorentzian shaped power spectrum at low to high freq.
  - ➡ slowly decaying ACF, with long decorrel. timescale
- **with frictional rigid lower boundary**
  - ➡ near exponential power spectrum at high freq.
  - ➡ ACF exhibits distinct timescale behav., faster decay
- **with additionally weakly red forcing (τ = 1 day)**
  - ➡ increased slope of near exponential power spectrum
  - ➡ ACF decays slower at very short lags

- variance of full solution at z = 5 km
  - ➡ almost entirely expl. by barotr. comp.

- ACF of barotropic comp. with frictional rigid lower boundary and weakly red forcing (thin black in Fig. 5c)
  - ➡ virtually identical to observed winter NAM ACF (as presented by Osprey and Ambaum, 2011, GRL)
- However, ACF of full solution changes shape across trop. levels, specifically
  - ➡ ratio of fast to slow component decreases with height – in contrast to observed NAM ACF
- Baroclinic eddy feedback may be expected to quickly remove baroclinic zonal mean flow component
  - ➡ although not clear how the associated additional forcing would further impact the ACF structure
- Also, phase spectrum (between forcing and zonal mean response) differs from the observed one
  - ➡ exhibits secondary minimum at intermed. freq. (cf. Fig. 3b,c), but incr. monotonically in observations

## 4. Conclusions & Outlook

- Dynamics of zonal mean secondary circul. contrib., to some extent, to obs. NAM spectral/ACF structure
- However, discrepancies in terms of vertical structure and phase relationship
  - ➡ resolved possibly by additional effect of eddy feedb. – neglected here, but known to exist in atmosph.
- Investigate actual relevance of above mechanism for observed annular variability in the troposphere
  - ➡ apply QG inversion method (K&G 2013, JAS) to check consist. of ERA-40 NAM forc. with above mech.